Potential groundwater recharge during floods

Paulo A. Herrera

Consultant on Water Resources, Santiago, Chile

paulo.herrera.ricci@gmail.com, corresponding author

Peter C. Lichtner

Adjunct Professor, U. New Mexico, Alburquerque, USA

peter.lichtner@gmail.com

Peer review status:

This is a non-peer-reviewed preprint submitted to EarthArXiv.

Potential groundwater recharge during floods

Paulo A. Herrera*[1] and Peter C. Lichtner†[2]

[1]Consultant on Water Resources, Santiago, Chile

[2]Adjunct Professor, U. New Mexico, Alburquerque, USA

February 16, 2026

*paulo.herrera.ricci@gmail.com. Corresponding author.
†peter.lichtner@gmail.com

Abstract

Groundwater constitutes 30% of fresh water reserves on Earth. It is important as a source for drinking water and irrigation due to its good quality. For many aquifers in arid regions, long-term groundwater extraction has put in risk its sustainable use. Thus, it is relevant to understand and quantify processes that contribute to sustainable groundwater recharge.

Most recharge to aquifers in arid regions occurs during flood events that happen with a frequency of a few years to decades. Paleo-climatic records show that intensity and frequency of floods have been particularly variable during periods of climate change. Therefore, understanding how floods could impact the magnitude and occurrence of groundwater recharge to aquifers in arid regions is relevant for improving water management strategies and assessing aquifer vulnerability to pollution from surface streams.

Direct measurement of infiltration during flood events is difficult, so it is common to complete analyses with numerical simulations. We present results of detailed numerical simulations of infiltration through the vadose zone during flood events. We use the results of the simulations to characterize infiltration patterns and quantify potential for recharge to aquifers considering different subsurface conceptualizations, from simple homogeneous to more realistic multi-scale heterogeneous sediment distributions. We also make a few additional general comments for practical applications.

keywords: water resources, groundwater recharge, flooding, numerical simulations, vadose zone

1 Introduction

It is known that the interaction between surface water and groundwater is a key process in hydrological systems that, among other things, serve to dampen floods and store water in aquifers for future use [8]. Groundwater is a main source of good quality water in many regions around the world, being approximately a third of the fresh water reserves on Earth [8]. It can be the sole water source in arid and semi-arid areas, i.e. regions with a ratio of mean annual rainfall to potential evapotranspiration less than 0.5 [32], which cover more than 30% of the Earth surface. Approximately a quarter (2.5 billion) of the world population lives in arid or semi-arid areas [14], reaching almost 100% in large geographic regions such as the Middle East, Southwest USA, and some places in Australia and South America, e.g. Southern Peru, Eastern Argentina and Northern Chile.

According to a report prepared by the United Nations published in 2026 [24]: *"Groundwater now provides about 50% of global domestic water use and over 40% of irrigation water, tying both drinking water security and food production directly to rapidly depleting aquifers. Around 70% of the world's major aquifers show long-term declining trends"* [24]. On the other hand, it is expected that due to climate change, dry periods (droughts) will have longer duration, so that demand for groundwater for use in irrigation and human consumption will increase [37]. It has been estimated that over 1.8 billion people lived under drought conditions in 2022–2023 and that the cost of those climatic anomalies amounted to about US$307 billion per year worldwide [24].

Intense groundwater exploitation is relatively recent, dating back only to the past century (early to mid 1900s). Therefore, there is a lack of a good understanding of long-term decades long dynamic behavior of aquifers under intense groundwater extraction, which is essential to assess sustainable water management strategies. Due to this, the use of numerical models to evaluate the dynamic response of aquifers to groundwater extraction is a common practice [5, 4]. Such models must take into account not only the complex nature of the sediments and rocks that compose aquifers, but also the fluctuating nature of climatic variables such as rainfall, temperature and evapotranspiration, which are the key elements to calculate the potential excess water available to recharge aquifers.

A common paradox in arid regions is that by definition, the calculation of potential recharge based on mean annual values of rainfall and evapotranspiration extracted from short time series up to few decades long predicts zero recharge. Hence, it has been postulated and demonstrated for some arid regions that currently available groundwater was recharged long ago during periods of different climatic patterns with higher rainfall and/or lower evapotranspiration [40]. For example, chemical analysis of vertical water sample profiles in North Africa indicate that concentrated recharge beneath streams ceased about 5,000 years ago as result of a shift in climate patterns [32]. Geochemical analysis of water samples from aquifers located in arid areas in

Texas and Nevada, USA, that experience low rainfall, estimated long residence time for pore water stored in unsaturated zone of the order of 50,000 to more than 100,000 years even at relatively shallow depth (≈ 25 m) [40]. Flash floods are rapid (within a few hours) and significant (of the order of up to ten times) increases in flow discharge of natural streams that are usually accompanied by the inundation of large land areas over river banks [1]. According to existing records, frequency and magnitude of floods have shown to be specially variable during periods of climate change [10, 40]. An alternative hypothesis postulates that most recharge to aquifers in arid regions happens during flash floods that take place periodically interspersed by a few to tens years [32, 37, 22, 11]. Available water for infiltration, i.e. recharge, during such events is several orders of magnitude higher than computed with mean annual values [20]. For example, a detailed review of recharge estimates in a semi-arid region located in New Mexico, USA; assessed that, while distributed recharge is usually less than 50-100 mm per year, focused recharge rate beneath streams can reach up to more than 700 m/year [32]. Focused recharge also results in much lower transit time of water through the unsaturated zone than for distributed recharge. The later can take up to a few centuries to travel from the ground surface to the water table in places where this locates a significant depth (≥ 100 m) [32].

The interaction between surface streams and shallow aquifers can be stronger during floods. For example, a site-specific study found based on observations and numerical simulations that for an aquifer located in Australia connected to a stream, groundwater levels could increase very rapidly and significantly (up to almost 10 m) during high river stages, while infiltrated water could travel significant distances away from streams (up to 40 m) within short time [41]. They also found rapid variations in groundwater flow direction before, during and after flooding events.

It is widely accepted that for most major exploited aquifers, long-term water use has exceeded renewable inflows and safe depletion limits, putting in risk the sustainable use of those resources for future generations [24]. Understanding how more intense floods can impact the interaction between ephemeral surface streams and groundwater can be useful for improving water management and flood mitigation systems [37, 22, 6]. It can also be relevant to evaluate potential increase in aquifer vulnerability due to intense recharge produced by natural floods or by dam failures during such events [7, 2, 43, 24].

The measurement of exchange fluxes between surface streams and aquifers through direct methods: stream-flow based, groundwater based and infiltration based; is difficult, particularly in arid regions where most streams are ephemeral and stay dry during long periods that are separated by extreme peak flow events [34]. Because of the difficulties to directly measure infiltration, it is also common to use analytical estimates or numerical simulations to complement observations [6, 33].

The principal objective of this work is estimating the potential for groundwater recharge to aquifers located in arid regions during flash floods. Specifically, we investigate the interaction between surface water and groundwater during flash flood events based on numerical simulations. We evaluate different plausible subsurface settings, from simple homogeneous materials to multi-scale heterogeneous sediment distributions. We use the simulation results to analyze the dynamic response of groundwater levels under focused recharge that may occur during floods. Based on those results we make conclusions for practical applications such as: estimating recharge from observed variations in groundwater levels, quantification of potential recharge for different flood durations and estimates for transit times of infiltrated water through the vadose zone.

2 Numerical simulations: Setup

We use numerical simulations for understanding the dynamics of recharge during flood events and assessing its potential magnitude. We employ a numerical simulator developed for use in supercomputers, PFLOTRAN [17], to perform detailed simulations of unsaturated flow through the vadose zone as result of focused recharge induced by floods. The use of numerical simulations for investigating stream-aquifer interaction have been applied in other studies [e.g. 9, 35, 6].

Infiltration during floods is controlled by many parameters, e.g.: permeability, heterogeneity of the subsurface, stream water height, depth to the water table and riverbed conductance [35, 6, 18]. Here, we focus only on a few of those parameters: magnitude and spatial distribution of permeability, vertical extent of the receiving aquifer because of the possibility of flow through the bottom boundary, and stream water height.

For the purpose of the analysis, we consider an idealized system composed of an ephemeral river that during flood events, has a river stage that can be considered almost constant and covers a well defined discharge section. In addition, we assume that the water table is relatively deep so that the river system is disconnected from the aquifer most of the time, which is the situation found in most ephemeral systems located in arid or semi-arid regions. The idealized system assumes that the riverbed is almost flat so that flow fluctuations due to micro-topography or vegetation can be neglected [39, 3]. In addition, we assume that the sediments beneath the riverbed are unconsolidated and that do not exhibit large fractures or cavities due to dessication or karstic processes [22]. Since we consider floods with peak discharge that can be ten times higher than the average, we assume that fine sediments deposited during low discharge are removed, so that the effective vertical hydraulic conductivity during peak flow does not depend on that layer [6]. As an additional simplification, we do not consider the potential presence of cobbles or boulders in the riverbed as observed in some rivers that experience high energy floods, e.g. the San José River located in northern Chile (Figure 1), which we used as motivation for the setting of the simulations.

Figure 1: Riverbed of San Jose river in northern Chile. Riverbed (top) and shallow stratigraphy (bottom). Picture taken from Undergraduate Thesis, G. Jimenez, U. Chile.

Neglecting rapid connection between the stream and the water table during floods, which is a reasonable assumption for deep water table aquifers [35]; infiltration rates can be considered almost constant during flooding events, discounting a short initial period of higher infiltration due to the sudden wetting of the dried upper sediments [29]. Large floods can carry enough water to keep a significant water height above the riverbed, so that discounting preferential flow through the stream due to high slope of the river bottom or low permeability of the riverbed, the infiltration problem transitions from one controlled by flow rates to one controlled by a quasi-constant hydraulic head boundary [13].

We consider three different permeability distributions for the sediments beneath the riverbed: homogeneous, stratified/layered and random spatially correlated. Similar distributions have been used in multiple studies to investigate groundwater dynamics [e.g. 26, 12, 15, 28, 31, and references therein]. Sediments correspond to two types of sandy soils, hereafter referred to as hydrofacies, materials or units, that were characterized as part of the assessment of an artificial recharge project in northern Chile (see Appendix for details). We refer to them as *Sandy* and *Silty*, for the coarser more permeable and the finer less permeable unit, respectively. This conceptualization based on two hydrofacies is reasonable to model a real site. For example, it is similar to the one adopted for the highly studied Hanford Site in the USA [36].

We model a cross-section 500 m wide and 80 m height that does not include slope for the riverbanks (Figure 2), and a water table located at 60 m depth. The 2D cross-section was divided into 20 cm wide and 5 cm high cells, resulting in a total of 4 million cells. Such discretization was chosen to guarantee a good numerical resolution and accuracy, while keeping the running time reasonable. The simulations were run in an instance of Amazon AWS with 72 computational cores and 192 GB RAM.

We analyse a single flood with a duration equal to 4 days, and we further simplify the problem by assuming a constant mean water stage. Thus, infiltration from the river was modeled as a constant pressure boundary condition applied along a central 20 m wide strip. Lateral flow through the saturated section of the aquifer was modeled using two hydrostatic pressure boundary conditions available in PFLOTRAN. The bottom boundary condition was modeled as an open (hydrostatic pressure) or no flow condition, which allows assessing the impact that the conceptualization of the aquifer geometry may have on the simulation results. Table 1 summarizes the simulations setup.

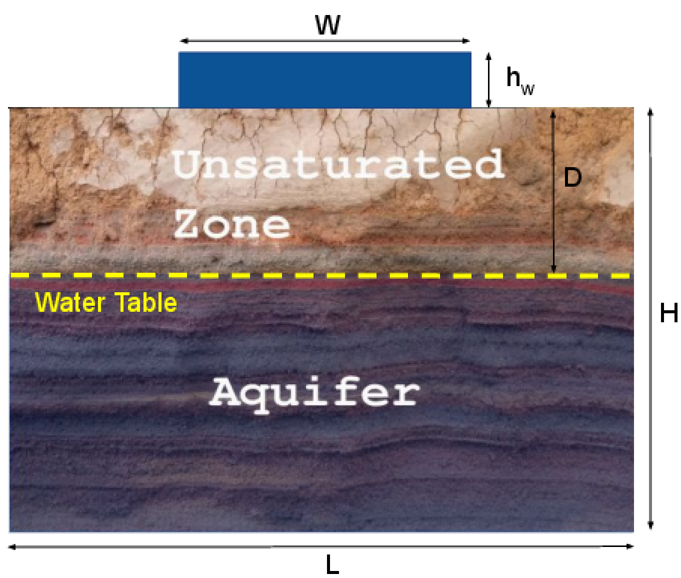

Figure 2: Schematic of cross-section considered in numerical simulations.

Parameter	**Value**	Symbol
Stream width [m]	20	W
Water height in stream [m]	1,0.5,0.2,0.1	h_w
Water table depth [m]	60	D
2D cross-section width [m]	500	L
2D cross-section height [m]	80	H
Hydrofacies	Sandy, Silty	-
Hydraulic conductivity [m/d]	7, 0.3	$\mathtt{K}$
Permeability [m^2]	8×10^{-12}, 3×10^{-13}	k
Porosity [-]	0.33, 0.46	ϕ

Table 1: Parameters used to set up simulations.

We simulate a total of 8 scenarios depending upon the stratigraphy of the sediments beneath the riverbed. As first scenario, we consider an aquifer composed of a single hydrogeological unit with a permeability equal to the mean value for the Sandy or Silty units (scenarios H1, H1b and H2). The next two scenarios were defined to account for the potential presence of low permeability units beneath the riverbed, which can contribute to the occurrence of unsaturated areas beneath even permanent surface streams due to reductions in vertical infiltration rates [33]. We consider stratified aquifers composed by two hydrogeological units: Sandy-Silty or Silty-Sand according to their vertical occurrence (scenarios L1 and L2). Silty layers 3 m thick are intercalated within higher permeability Sandy layers 10 m each. This sequence is repeated from the ground surface to the bottom of the domain. To better quantify the impact of river depth on infiltration rates, three additional scenarios similar to L2 were considered for which the river stage was set to: 0.5 (L2b), 0.2 (L2c) and 0.1 (L2d) meters instead of the 1.0 m used for the original L2 scenario.

Finally, for the last 4 scenarios, we consider a sandy aquifer with values of permeability distributed according to a random multi-scale spatially correlated field [12, 15, 28, 31]. We use a multi-scale approach to generate bimodal gaussian correlated fields by using an implementation of the Turning Bands method [25, 38]. First, we generate random fields with different ratios between horizontal (λ_h) to vertical (λ_v) correlation lengths, that we use as basis to create hydrofacies distributions using an indicator approach [16]. The resulting hydrofacies distribution exhibits good continuity and the same spatial correlation or extension described by the correlation lengths of the underlying random field. Second, we generate additional random fields with mean permeability equal to the one assigned to each hydrofacies and short isotropic correlation lengths equal to 0.5 m. For all the *intra-facies* permeability distributions we consider an exponential covariance model and low variance σ_Y equal to 0.5 ($Y = Ln(k)$), which corresponds to relatively mild heterogeneity for real aquifers [15, 31]. These secondary random fields were used to assign saturated permeability values to each cell of the domain. The resulting overall permeability field has a bimodal distribution and multiple correlation lengths, which are properties that have been postulated as more realistic [15, 16, 28, 31]. For example, Figure 3 shows the hydrofacies distribution and multi-scale permeability field assigned to scenario R3. Table 2 summarizes the simulated scenarios.

Run	Description
H1$^+$	Homogeneous sandy aquifer
H2	Homogeneous silty aquifer
L1	Layered aquifer: sandy/silty
L2*	Layered aquifer: silty/sandy
R1	Random correlated permeability, with $\lambda_h/\lambda_v = 1$
R2	Random correlated permeability, with $\lambda_h/\lambda_v = 10$
R3†	Random correlated permeability, with $\lambda_h/\lambda_v = 20$
R4	Random correlated permeability, with $\lambda_h/\lambda_v = 40$

Table 2: Parameters used to characterize geological settings. In all simulations with gaussian distributions we considered the vertical correlation length $\lambda_v = 3$ m and a proportion distribution of 0.23 and 0.77 for the Silty and Sandy units, respectively. $^+$H1b equal to H1, except that bottom boundary condition is set to no flow. *L2b,c,d equal to L2 but with different river stage. †R3b equal to R3 except that a single value of permeability is assigned to each hydrofacies.

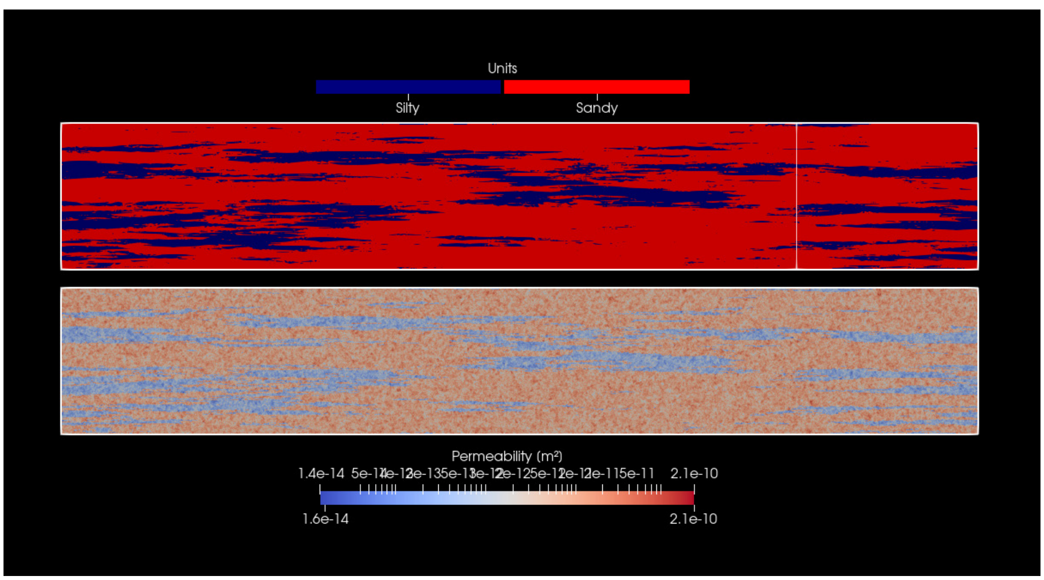

Figure 3: Hydrofacies distribution and multi-scale random permeability distribution assigned to scenario R3.

We use a pair of constitutive relations to characterize the unsaturated flow properties (see Appendix for details), which were tied to each hydrofacies. This is a reasonable assumption given that each hydrofacies is supposed to have a single characteristic grain size distribution [23].

3 Numerical simulations: Results

3.1 Saturation distribution

Figure 4 presents the simulated saturation distribution along a vertical cross-section after 4 days of infiltration through the riverbed for the 8 main scenarios considered. There are major differences in the saturation distributions for the different scenarios.

The homogeneous (H1 and H2) and layered (L1 and L2) scenarios show a wetting front with a relatively simple shape. The speed of the advancing front for those scenarios is mainly controlled by the different values of permeability assigned to both hydrofacies (Sandy and Silty). For the layered scenarios, the Silty layers acts as low permeability barriers generating a so called *leaky-flow*, i.e. partially-saturated permeable sediments underneath fully saturated pockets or perched aquifers.

The saturation distribution for the scenarios with multi-scale permeability, R1 to R4, shows the development of a saturation front beneath the riverbed with a complex pattern and a mean width that is controlled by the correlation length assigned to the less permeable hydrofacies. The front is narrow for scenario R1 that consider a short horizontal correlation length, while it becomes wider for the scenarios with longer horizontal correlation (R3 and R4). The inclusions of low permeable Silty material act as barriers for vertical flow, so that water accumulates on top of them and spills over their flanks. Just below the riverbed and up to a certain variable depth, there is a well connected fully saturated central zone. However, the distribution of saturation becomes erratic and highly non-uniform at greater depth. This means that for practical applications point-like observations, e.g. core samples or water samples obtained through lysimeters, may not provide enough information to characterize the saturation distribution. Interestingly, even if the fully saturated front does not reach the original water table for the time period considered, there is clear local mounding below zones with higher leakage, e.g. left central and central zones for Scenarios R3 and R4, respectively. However, the height of the mounding is variable even within relatively short distances, which may be an obstacle to correctly infer recharge rates from water level measurements as it is common practice in hydrogeological studies.

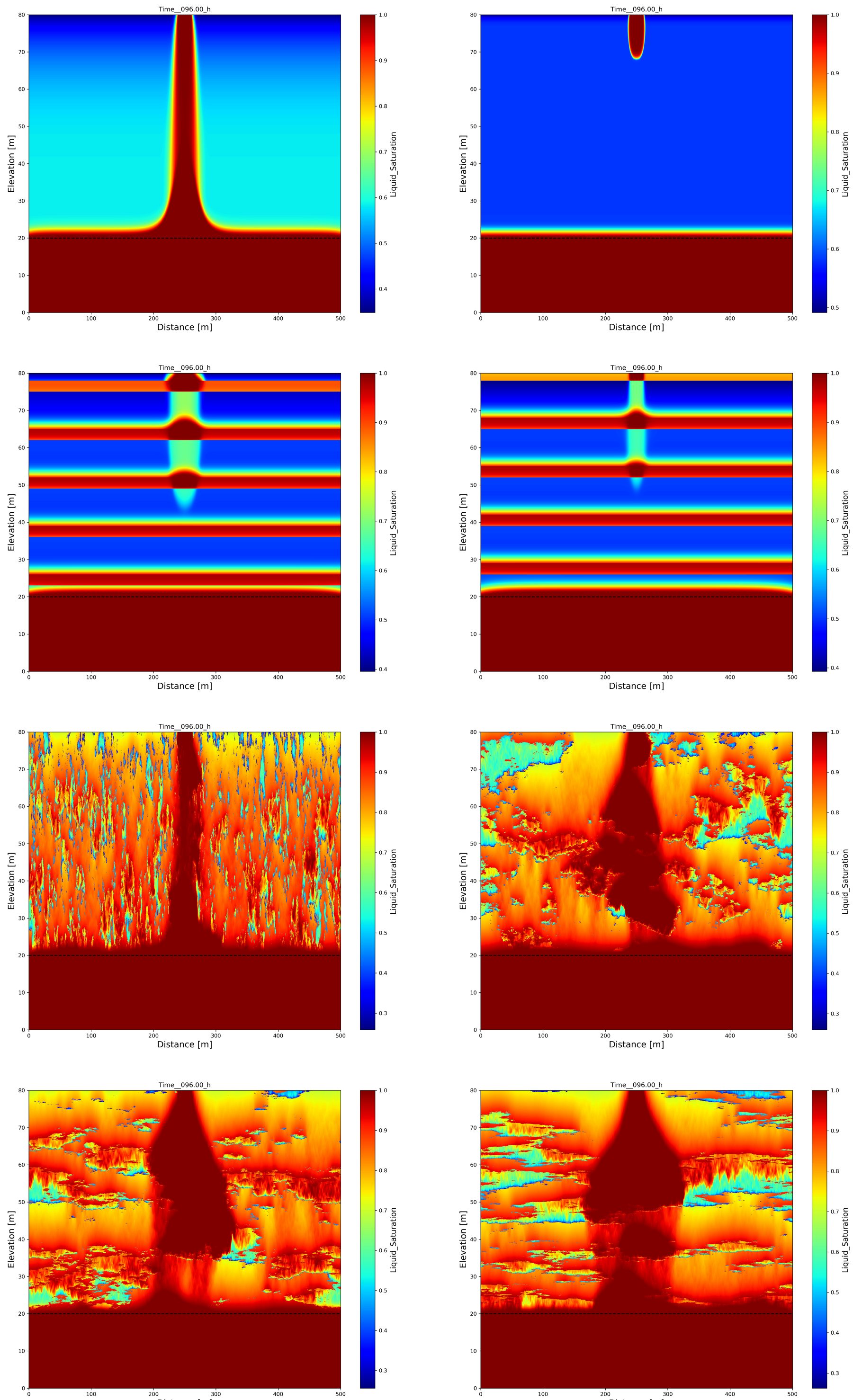

Figure 4: Simulated saturation after 96 hrs of infiltration along a cross-section located beneath the riverbed. River centerline located at 250 m in the horizontal axis. From left to right and top to bottom: H1, H2, L1, L2, R1, R2, R3 and R4.

Figure 5 shows simulated saturation at the end of the 4 days for Scenarios R3 and R3b, thus it allows assessing the impact of including *intra-facies* heterogeneity. There are only small differences that are almost undistinguishable in the figure, which indicates that the saturation distribution is mainly controlled by the distribution of the hydrofacies, i.e. large-scale heterogeneity.

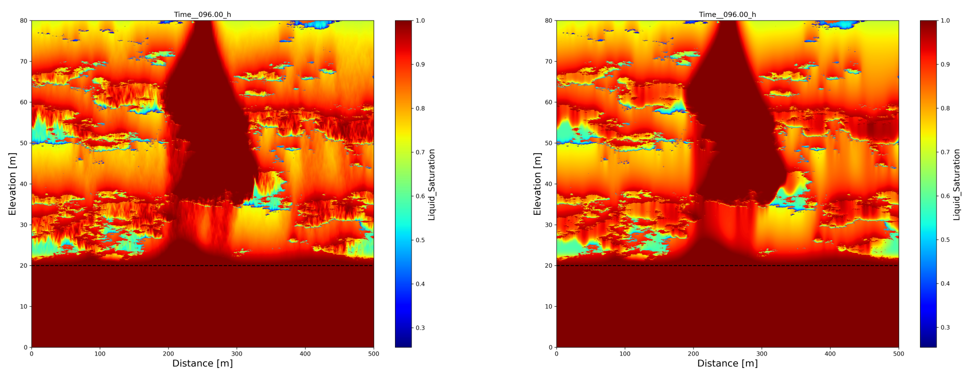

Figure 5: Simulated saturation after 96 hrs of infiltration for R3 (left) and R3b (right).

In all scenarios discussed so far, we considered a permeable boundary condition at the bottom of the receiving aquifer. Hence, there is potential for a large part of the water that reaches the main aquifer to leave the domain through the bottom. Figure 6 shows a comparison between Scenario H1b that includes a no-flow bottom boundary condition and the reference Scenario H1, which considers an open bottom boundary. There is a large difference in the wetting front that develops below the riverbed for both scenarios. For Scenario H1b, water can only leave the domain though the lateral faces, so that there is significant rise of the original water table within the central part of the model domain for accommodating lateral flow to balance the inflow due to recharge. This distinction can be potentially important to infer the existence of lower impermeable limits based on the observation of changes in groundwater levels during and after flood events. On the other hand, this difference can lead to errors in the interpretation of observed mounding for estimating recharge rates. The infiltration for both scenarios, R3 and R3b, is the same (see Table 3) despite the large differences observed in the shape of the water table.

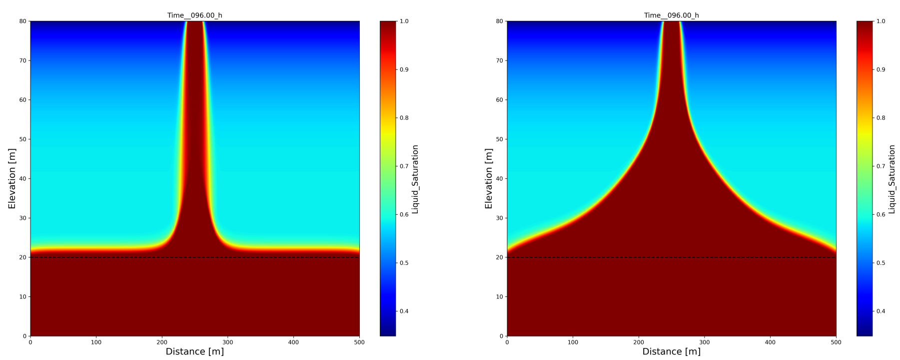

Figure 6: Simulated saturation after 96 hrs of infiltration for H1 (left) and H1b (right).

3.2 Water table variation

Figure 7 shows simulated piezometric head at the end of the simulated 4 days, along a horizontal profile located at the original position of the water table at z=20 m (60 m deep). Most of the simulated scenarios show a significant increase of the water table in the central zone of the domain beneath the river bed. The magnitude of the change is particularly important for Scenario H1b that considers no-flow through the bottom of the domain. The increase in piezometric levels is also important for the most permeable homogeneous scenario (H1) and all scenarios that consider heterogeneous sediments (R). For the latter, the variation in piezometric head along the profile is irregular, reaching a maximum at some location near the center of the domain, but not at the center as in the scenarios with homogeneous or layered materials. This can be potentially important for practical applications that require the interpretation of observed groundwater levels at a single or few boreholes.

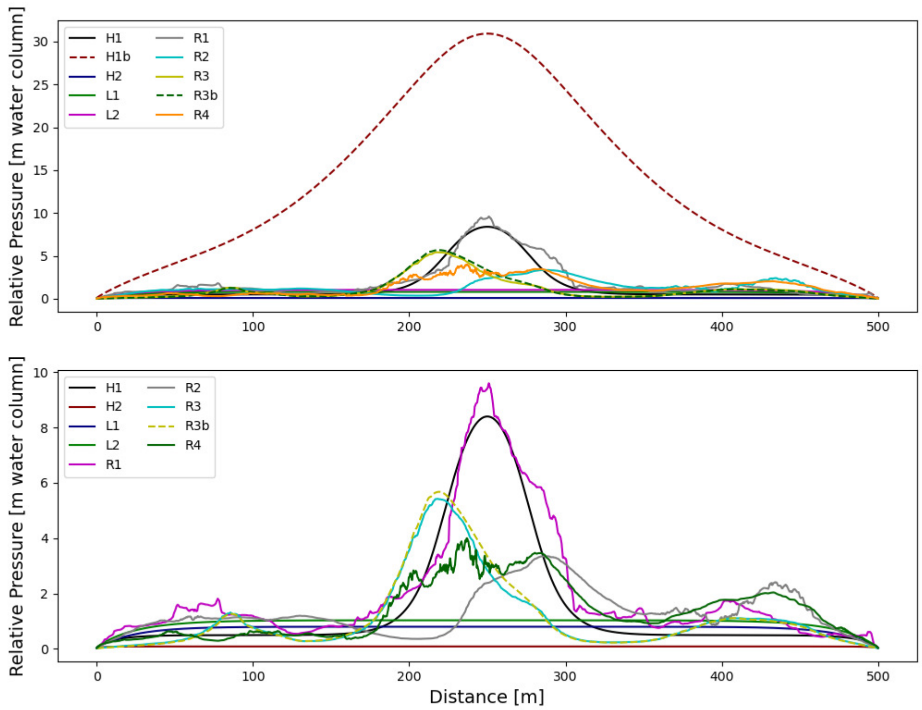

Figure 7: Simulated change in piezometric head along a horizontal profile at z=20 m, i.e. initial water table position. Maximum increases in piezometric head for different scenarios expressed as meters of water column are: 8.4(H1), 30.9(H1b), 0.1(H2), 0.8(L1), 1.0(L2), 9.6(R1), 3.4(R2), 5.4(R3), 5.7(R3b) and 4.0(R4). Bottom plot is similar to the top one, except for H1b results.

3.3 Infiltration rates

Figure 8 shows simulated infiltration rates through the riverbed. As predicted by existing theory, the infiltration rate decreases asymptotically from an initial peak value to a final constant value determined by the hydraulic gradient controlled by the simulated river stage and the saturated hydraulic conductivity. The final simulated infiltration rate through the 20 m wide riverbed ranges between 0.1 to 2.4 L/s per meter of the river section (Table 3). The time to reach the final value is short for the homogeneous and layered scenarios, but it is significantly longer ($\geq$ 20 hours) for the cases that consider heterogeneous sediments. The exception to the previous statement is Scenario H1b (no flow bottom boundary) that shows a late deviation in infiltration as result of hydraulic control from the outflow boundaries.

As expected, the highest infiltration rate corresponds to the scenario with homogeneous Sandy subsurface and the lowest to the scenarios where vertical water flow is controlled by the occurrence of the Silty unit. The scenarios with heterogeneous sediments have intermediate values of infiltration rate, which can be explained by the presence of cells with values of saturated permeability that are higher and/or lower than the mean value assigned to each hydrofacies.

It is useful for the interpretation of the final infiltration rates to convert them to equivalent distributed recharge as computed for rainfall. Assuming a 5 km wide valley, the final infiltration rates are equivalent to an areal distributed recharge of up to 160 mm, with a mean value between 60 to 80 mm. Such equivalent recharge must be compared to the mean annual rainfall recorded in arid regions where ephemeral streams occur, which is usually less than 100 mm/year for semi-arid areas and even less for arid regions, e.g. less than 5 mm/year in the case of the lower section of the San José River valley in northern Chile. Therefore, the potential recharge to the groundwater during a single flood event can be significant for aquifers in arid regions.

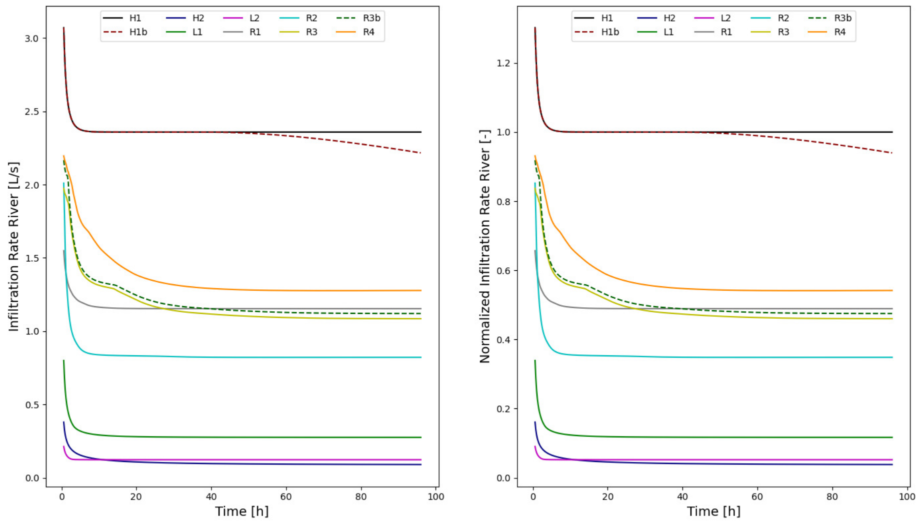

Figure 8: Simulated infiltration rate across the 20 m wide riverbed versus time.

The results of the simulations show that the water table rise due to focused recharge is not necessarily correlated with infiltration rates. For example, Scenarios H1 and H1b have similar final infiltration rates (2.4 and 2.2 L/s), but quite different maximum increases in water table: 8.4 and 31.0 m, respectively. On the other hand, final infiltration rates for the scenarios with heterogeneous sediments show low variability, ranging between 0.8 to 1.2 L/s. However, the water table increase is significantly higher for Scenario R1 (9.6 m) in comparison to the other three with increases between 3.4 and 5.7 m. This calls for caution when estimating recharge rates from observed variations in groundwater levels.

Assuming a constant river depth during a flood is a simplifying assump-

Run	Final Vertical Infiltration [m/d]	Final Infiltration [L/s/m]	Total Infiltration in 96 hrs [m^3/m]	5 km†	10 km†	20 km†	Equivalent distributed recharge (mm)
H1	10.20	2.36	816	4.1	8.2	16.3	163
H1b	9.59	2.22	767	3.8	7.7	15.3	153
H2	0.39	0.09	31	0.2	0.3	0.6	6
L1	1.21	0.28	97	0.5	1.0	1.9	19
L2	0.52	0.12	41	0.2	0.4	0.8	8
R1	4.97	1.15	397	2.0	4.0	7.9	79
R2	3.54	0.82	283	1.4	2.8	5.7	57
R3	4.67	1.08	373	1.9	3.7	7.5	75
R3b	4.84	1.12	387	1.9	3.9	7.7	77
R4	5.53	1.28	442	2.2	4.4	8.8	88

Table 3: Final vertical infiltration rate and total infiltration and equivalent distributed infiltration rate assuming a 5 km wide valley. †Columns show total infiltration volume in million cubic meters for river sections of different length.

tion, since a flood usually consists of two stages: a raising water level period, followed by one of declining water elevation. Nevertheless, ready water availability is the factor that facilitates infiltration. Higher or lower water levels result only in minor changes in surface infiltration as the result of changes in hydraulic gradient given a higher hydraulic head below the river bed. For example, Table 4 reports the final infiltration rate for Scenario L2 as a function of river stage. These results demonstrate that decreasing the river depth by a factor of 10 produces a $\sim$30% decrease in infiltration rate.

Run	River Depth [m]	Final Infiltration Rate [L/s/m]
L2	1.0	0.12
L2b	0.5	0.10
L2c	0.2	0.09
L2d	0.1	0.08

Table 4: Total infiltration rate considering different river depths.

The analysis we present is based on 2D simulations, it is likely that infiltration for a 3D setting would be higher because of the extra degree of freedom for the infiltrated water to flow [19] or, a higher connection of fast flow pathways in heterogeneous sediments [21].

4 Conclusions

Based on the results of numerical simulations that considered a few variations of a unique disconnected aquifer, we can make the following general statements about aquifer recharge in arid regions during flooding events that usually occurred with a few years to decades return period:

1. The recharge that may occur during a few days duration event can be significant, of the order of a few times the typical mean annual precipitation registered in those regions. This could explain estimates for recent/modern recharge to aquifers located in arid regions where excess water calculated from mean rainfall and evapotranspiration is negligible or zero.

2. Transit times of infiltrated water during focused recharge events, even for aquifers with relatively deep water table ($\geq$ 50 m), can be short, of the order of a few hours. This must be considered when evaluating potential groundwater pollution due to infiltration of poor quality water as results of spills to surface streams or dam failures, e.g. tailings dams located on or near surface streams.

3. Infiltration patterns during focused recharge, as it occurs during flooding events, may be quite complex to analyze or model for real settings. In particular, numerical simulations that rely on simple representations of the subsurface sediments stratigraphy can provide estimates of recharge, saturation distribution, water table mounding and transit times to the water table; that can be misleading. Therefore, results of such simulations should be used with caution when evaluating water management options or aquifer vulnerability to pollution.

4. The complexity of the saturation patterns observed under more realistic assumptions, e.g. multi-scale heterogeneous sediments, may be quite difficult to interpret based on a few point-like measurements such as core samples or water samples taken from cup lysimeters.

5. Estimates of recharge based on water level rise, which relies on the concept of specific yield or storage coefficient, may be bogus due to incorrect assumptions about the distribution of the infiltrated water and/or shape of the resulting wetting front.

6. Different boundary conditions, e.g. permeable or impermeable bottom boundary, may produce large differences in results of numerical simulations of this type of processes. This should be considered as a source of uncertainty in studies that rely on the use of numerical models. Moreover, the presence of that type of boundary conditions in real aquifers should be considered when analyzing field collected data, e.g. piezometric head for estimation of recharge rates.

Acknowledgements

The authors are grateful to Glenn Hammond, lead developer of PFLOTRAN, who provided useful comments to early drafts and support for the setup of the numerical simulations.

References

[1] K. Ali, R. M Bajracharyar, and N. Raut. Advances and challenges in flash flood risk assessment: A review. *Journal of Geography & Natural Disasters*, 7(2):1–6, 2017.

[2] M. Ascott, D. Lapworth, D. Gooddy, R. Sage, and I. Karapanos. Impacts of extreme flooding on riverbank filtration water quality. *Science of the Total Environment*, 554:89–101, 2016.

[3] E. Bonanno, G. Blöschl, and J. Klaus. Discharge, groundwater gradients, and streambed micro-topography control the temporal dynamics of transient storage in a headwater reach. *Water Resources Research*, 59(7):e2022WR034053, 2023.

[4] J.D. Bredehoeft. The water budget myth revisited: Why hydrogeologists model. *Groundwater*, 40(4):340–345, 2002.

[5] J.D. Bredehoeft, S.S. Papadopulos, and H.H. Cooper. Groundwater: The water budget myth. *Scientific Basis of Water Resource Management*, 51:57, 1982.

[6] P. Brunner, R. Therrien, P. Renard, C.T. Simmons, and H.H. Franssen. Advances in understanding river-groundwater interactions. *Reviews of Geophysics*, 55(3):818–854, 2017.

[7] D.A. Cenderelli et al. Floods from natural and artificial dam failures.

Inland Flood Hazards: Human, riparian and aquatic communities, pages 73–103, 2000.

[8] V.T. Chow, D.R. Maidment, and L.W. Mays. *Applied Hydrology*. McGraw-Hill, 1988.

[9] J. Constantz, A.E. Stewart, R. Niswonger, and L. Sarma. Analysis of temperature profiles for investigating stream losses beneath ephemeral channels. *Water Resources Research*, 38(12):52–1, 2002.

[10] P.G. Cook, W.M. Edmunds, and C.B. Gaye. Estimating paleorecharge and paleoclimate from unsaturated zone profiles. *Water Resources Research*, 28(10):2721–2731, 1992.

[11] M.O. Cuthbert, R.I. Acworth, M.S. Andersen, J.R. Larsen, A.M. McCallum, G.C. Rau, and J.H. Tellam. Understanding and quantifying focused, indirect groundwater recharge from ephemeral streams using water table fluctuations. *Water Resources Research*, 52(2):827–840, 2016.

[12] G. Dagan. *Flow and transport in porous formations*. Springer-Verlag, 1989.

[13] G.A. Fox and D.S. Durnford. Unsaturated hyporheic zone flow in stream/aquifer conjunctive systems. *Advances in Water Resources*, 26(9):989–1000, 2003.

[14] M.K. Gaur and V.R. Squires. Geographic extent and characteristics of

the world's arid zones and their peoples. In *Climate variability impacts on land use and livelihoods in drylands*, pages 3–20. Springer, 2017.

[15] L.W. Gelhar. *Stochastic subsurface hydrology.* Prentice-Hall, 1993.

[16] J. Gómez-Hernández and X. Wen. To be or not to be multi-gaussian? A reflection on stochastic hydrogeology. *Advances in Water Resources*, 21(1):47–61, 1998.

[17] G.E. Hammond, P.C. Lichtner, and R.T. Mills. Evaluating the performance of parallel subsurface simulators: An illustrative example with pflotran. *Water Resources Research*, 50(1):208–228, 2014.

[18] J. Hauser, F. Wellmann, and M. Trefry. Water table uncertainties due to uncertainties in structure and properties of an unconfined aquifer. *Groundwater*, 56(2):251–265, 2018.

[19] P.A. Herrera. Numerical simulations of saturated and unsaturated flow in porous media (*Simulaciones numéricas de flujo en medios porosos saturados y no saturados*). Undergraduate Thesis, Universidad de Chile, 2000.

[20] P.A. Herrera and P. Lichtner. Potential groundwater recharge during floods: First-order estimates. *Tecnologia y Ciencias Agua*, To appear, 2026.

[21] A.G. Hunt. Applications of percolation theory to porous media with

distributed local conductances. *Advances in Water Resources*, 24(3-4):279–307, 2001.

[22] H. Jourde, A. Lafare, N. Mazzilli, G. Belaud, L. Neppel, N. Dörfliger, and F. Cernesson. Flash flood mitigation as a positive consequence of anthropogenic forcing on the groundwater resource in a karst catchment. *Environmental Earth Sciences*, 71:573–583, 2014.

[23] X. Li, J.H. Li, and L.M. Zhang. Predicting bimodal soil–water characteristic curves and permeability functions using physically based parameters. *Computers and Geotechnics*, 57:85–96, 2014.

[24] K. Madani. Global Water Bankruptcy: Living beyond our hydrological means in the post-crisis era. Technical report, United Nations University Institute for Water, Environment and Health (UNU-INWEH), 2026. DOI: 10.53328/INR26KAM001.

[25] A. Mantoglou and J.L. Wilson. The Turning Bands method for simulation of random fields using line generation by a spectral method. *Water Resources Research*, 18(5):1379–1394, 1982.

[26] G. Matheron and G. de Marsily. Is transport in porous media always diffusive? A counterexample. *Water Resources Research*, 16(5):901–917, 1980.

[27] Y. Mualem. A new model for predicting the hydraulic conductivity of

unsaturated porous media. *Water Resources Research*, 12(3):513–522, 1976.

[28] S.P. Neuman and V. Di Federico. Multifaceted nature of hydrogeologic scaling and its interpretation. *Reviews of Geophysics*, 41(3), 2003.

[29] J. Philip. Theory of infiltration. In *Advances in Hydroscience*, volume 5, pages 215–296. Elsevier, 1969.

[30] L.A. Richards. Capillary conduction of liquids through porous mediums. *Physics*, 1(5):318–333, 1931.

[31] Y. Rubin. *Applied stochastic hydrogeology.* Oxford University Press, 2003.

[32] B.R. Scanlon, K.E. Keese, A.L. Flint, L.E. Flint, C.B. Gaye, W.M. Edmunds, and I. Simmers. Global synthesis of groundwater recharge in semiarid and arid regions. *Hydrological Processes*, 20(15):3335–3370, 2006.

[33] O.S. Schilling, D.J. Irvine, H.J. Hendricks Franssen, and P. Brunner. Estimating the spatial extent of unsaturated zones in heterogeneous river-aquifer systems. *Water Resources Research*, 53(12):10583–10602, 2017.

[34] M. Shanafield and P.G. Cook. Transmission losses, infiltration and groundwater recharge through ephemeral and intermittent streambeds: A review of applied methods. *Journal of Hydrology*, 511:518–529, 2014.

[35] M. Shanafield, P.G. Cook, P. Brunner, J. McCallum, and C.T. Simmons. Aquifer response to surface water transience in disconnected streams. *Water Resources Research*, 48(11), 2012.

[36] X. Song, X. Chen, M. Ye, Z. Dai, G. Hammond, and J.M. Zachara. Delineating facies spatial distribution by integrating ensemble data assimilationand indicator geostatistics with level-set transformation. *Water Resources Research*, 55(4):2652–2671, 2019.

[37] R. Taylor, B. Scanlon, P. Döll, M. Rodell, R. Van Beek, Y. Wada, L. Longuevergne, M. Leblanc, J. Famiglietti, M. Edmunds, et al. Ground water and climate change. *Nature Climate Change*, 3(4):322–329, 2013.

[38] A.F.B. Tompson, R. Ababou, and L.W. Gelhar. Implementation of the three-dimensional turning bands random field generator. *Water Resources Research*, 25(10):2227–2243, 1989.

[39] D. Tonina and J.M. Buffington. Hyporheic exchange in mountain rivers i: Mechanics and environmental effects. *Geography Compass*, 3(3):1063–1086, 2009.

[40] S.W. Tyler, J.B. Chapman, S.H. Conrad, D.P. Hammermeister, D.O. Blout, J.J. Miller, M.J. Sully, and J.M. Ginanni. Soil-water flux in the southern Great Basin, United States: Temporal and spatial variations over the last 120,000 years. *Water Resources Research*, 32(6):1481–1499, 1996.

[41] N.P. Unland, I. Cartwright, E. Daly, B.S. Gilfedder, and A.P. Atkinson. Dynamic river–groundwater exchange in the presence of a saline, semi-confined aquifer. *Hydrological Processes*, 29(23):4817–4829, 2015.

[42] M.Th. van Genuchten. A closed-form equation for predicting the hydraulic conductivity of unsaturated soils. *Soil Science Society of America Journal*, 44(5):892–898, 1980.

[43] A.M. Youssef, M.M. Abu-Abdullah, E.A. AlFadail, H.D. Skilodimou, and G.D. Bathrellos. The devastating flood in the arid region a consequence of rainfall and dam failure: Case study, Al-Lith flood on 23th November 2018, Kingdom of Saudi Arabia. *Zeitschrifft Für Geomorphologie*, 63:115–136, 2021.

Appendix

PFLOTRAN [17], available at https://pflotran.org/, simulates unsaturated flow solving the following form of Richards Equation [30]:

$$\frac{\partial}{\partial t}(\phi s \eta) + \nabla \cdot (\eta \mathbf{q}) = Q_w, \tag{A.1}$$

with porosity ϕ [m^3/m^3], saturation s [-], molar water density η [kmol/m^3], source/sink term Q_w [kmol/m^3/s], and Darcy flux $\mathbf{q}$ [m/s]

$$\mathbf{q} = -\frac{k k_r(s)}{\mu} \nabla (P - \rho g z) \tag{A.2}$$

where k is permeability [m^2], k_r is relative permeability [-], μ is dynamic viscosity [Pa s], P is pressure [Pa], ρ is mass water density [kg/m^3], g is gravity [m/s^2] and z is elevation. Solving (A.1) requires the definition of a couple of closure models for linking water content θ or saturation $s = (\theta - \theta_r)/(\phi - \theta_r)$, where θ_r is residual water content; to relative permeability and pressure or capillary pressure. Those relations are commonly referred to as unsaturated flow properties.

We considered the properties of two soils samples collected in sites in northern Chile considered in the past for implementing artificial recharge projects [19, and references therein] in the numerical simulations. One of the samples referred to as Silty, was collected near the lower section of the San José River Valley; while the second one (Sandy) was collected in a valley located 1000 km south, near de city of Copiapó. Both sites are located in fluvial-alluvial valleys in extreme arid areas: the mean annual rainfall in Arica is < 5 mm/yr and < 24 mm/yr in Copiapó according to data taken from the Climate Explorer at https://explorador.cr2.cl/.

The unsaturated flow properties of the samples were characterized through laboratory tests. The interpretation of the results considered the van Genuchten model for the water content versus suction relation [42],

$$\theta(h) = \theta_r + \frac{\theta_s - \theta_r}{[1 + |\alpha h|^n]^m} \tag{A.3}$$

and the Mualem model for relative permeability [27],

$$k_r(h) = Se^{0.5}[1 - (1 - Se^{1/m})^m]^2 \tag{A.4}$$

where $Se = \frac{\theta - \theta_r}{\theta_s - \theta_r}$ is known as residual saturation and $m = 1 - \frac{1}{n}$. Table A.1 summarizes the parameter values considered in the numerical simulations, while Figure A.1 shows the resulting curves.

Parameter	**Sandy**	**Silty**
Saturated water content, θ_s [-]	0.33	0.46
Residual water content, θ_r [-]	0.19	0.01
Inverse of entry pressure, α [Pa^{-1}]	4.9x10^{-5}	1.8x10^{-5}
Distribution index, n [-]	2.45	1.35
$m = 1 - 1/n$	0.59	0.26
Saturated hydraulic conductivity, K_{sat} [m/day]	7.0	0.3

Table A.1: Unsaturated flow parameters considered in the numerical simulations.

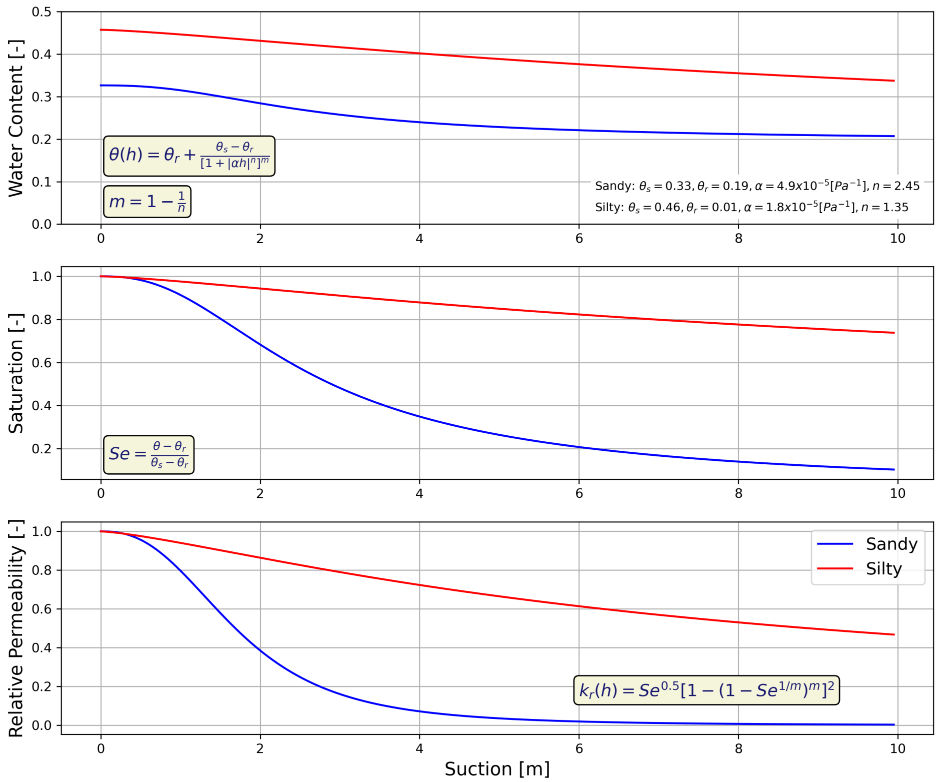

Figure A.1: Water retention and relative permeability for sandy and silty soils considered in numerical simulations [19].

Conflict of interests

The authors declare that they have no known competing financial interests or personal relationships that could have appeared to influence the work reported in this paper.

Author contribution

P.A.H. was in charge of initial conceptualization, numerical simulations and writing of initial draft; P.C.L. provided comments to conceptualization and review initial draft.